

VIP Very Important Paper



# Understanding the Effect of Polydopamine Interlayer on the Long-Term Cycling Performance of Silicon Anodes: A Multiphysics-Based Model Study

Williams A. Appiah,<sup>[a]</sup> Dohwan Kim,<sup>[a]</sup> Jihun Song,<sup>[a]</sup> Myung-Hyun Ryou,<sup>[b]</sup> and Yong M. Lee<sup>\*[a]</sup>

To understand the effect of a polydopamine interlayer between a copper current collector and a silicon composite electrode, a physics-based model is used to analyze the cycle performance of silicon-based lithium-ion half-cells with bare and polydopamine-treated copper current collectors. We investigate the capacity-fading mechanisms of the two cell configurations by analyzing the model parameters that change with cycling. The major capacity-fading mechanisms in the silicon-based anodes are the increase in film resistance (solid electrolyte interphase resistance and contact resistance) and the isolation of silicon

active material. The polydopamine interlayer reduced the contribution of the film resistance and isolation of the silicon active material to the capacity fade by 22% and 10%, respectively. The insulating-nature of the polydopamine interlayer resulted in an increase in the charge transfer resistance contributing to 15% reduction in the capacity retention. The efficacy of the physics-based model is validated with experimental data obtained from silicon-based half-cells with bare and polydopamine-treated copper current collectors.

## 1. Introduction

The replacement of commercial graphite anode material (theoretical capacity of  $372 \text{ mAh g}^{-1}$ ) with alternative anode materials of relatively higher theoretical capacity has been considered a promising solution to overcome the challenges related to energy and power densities that hinder the effective extension of lithium-ion batteries (LIBs) applications in electric vehicle and stationary energy storage systems.<sup>[1–4]</sup> As one of the most promising anode material candidates to be used in LIBs, silicon has a relatively higher theoretical specific capacity ( $3579 \text{ mAh g}^{-1}$ ) as well as other advantages such as environmental friendly and terrestrial abundance.<sup>[5–7]</sup> However, large volume expansion (up to 275%) of silicon during (de)lithiation processes<sup>[8]</sup> resulting in delamination of the composite electrode from the surface of the current collector, pulverization of silicon particles, formation of unstable solid electrolyte interphases (SEIs), and permanent capacity losses,<sup>[5,9–10]</sup> hinders the commercialization of silicon anode material for LIBs. To address these issues, the use of binding materials with stronger adhesion forces such as alginate, copolyimide, poly(acrylic acid) (PAA), carboxymethyl cellulose and polymers that form cross-linked networks have been widely investigated.<sup>[11–14]</sup> However, the mechanisms underlying the enhancement in the electro-

chemical performance by these binding materials are complicated and not well understood.

In addition, treating the surface of the copper current collector with a mussel-inspired polydopamine (PD) has proven to be a means of improving the electrochemical performance of silicon-based anode.<sup>[15]</sup> The improvement in the cycling and rate performance was attributed to the enhancement in the adhesion between the silicon composite material and the copper current collector preventing the delamination of the composite material from the surface of the current collector. A further analysis on the rate performance of silicon-based anode lithium-ion cells with a polydopamine treated copper current collector using mathematical model suggested that, the presence of the polydopamine reduces the contact resistance between the composite material and the copper current collector.<sup>[16]</sup> However, this analysis was not extended to the cycling performance because of the limited information on the capacity-fading mechanisms of silicon-based anodes with a polydopamine treated copper current collector. On the other hand, the poor cyclability of silicon-based electrodes are attributed to formation of cracks within the composite electrode,<sup>[17]</sup> loss of electrical contacts between silicon particles<sup>[18]</sup> at the current collector interface,<sup>[15,19]</sup> parasitic reaction between freshly exposed silicon and electrolyte leading to the formation of an unstable SEI owing to continuous electrolyte degradation products.<sup>[20–21]</sup> Nevertheless, the analytical and quantitative effect of the presence of the polydopamine thin film on the surface of the copper current collector on these capacity-fading mechanisms of silicon-based anodes are yet to be reported. The analyses and quantification of the role of the polydopamine interlayer on the degradation processes will improve the prediction of the cell capacity during operations.

The major issue is the non-destructive extraction of the capacity degradation mechanisms. To address this issue, two

[a] W. A. Appiah, D. Kim, J. Song, Prof. Y. M. Lee  
*Department of Energy Science and Engineering  
 Daegu Gyeongbuk Institute of Science and Technology (DGIST)  
 333 Techno Jungang-daero, Hyeonpung-myeon, Dalseong-gun, Daegu  
 42988, Republic of Korea  
 E-mail: yongmin.lee@dgist.ac.kr*

[b] Prof. M.-H. Ryou  
*Department of Chemical and Biological Engineering  
 Hanbat National University  
 125 Dongseo-daero, Yuseong-gu, Daejeon 34158, Republic of Korea*

non-destructive methods have been used to analyze the capacity-fading mechanism in lithium-ion batteries. The first method has to do with the analysis of the changes in voltage profiles with cycling. This involves the measurement of a close-to-equilibrium open-circuit voltage (OCV) to reflect thermodynamic state of charge ( $t$ -SOC), and incremental capacity analysis (ICA) to correlate the capacity fading with the estimated  $t$ -SOC.<sup>[22]</sup> This method has been used to provide a quantitative assessment of different capacity degradation mode through a diagnostic and prognostic model.<sup>[23–25]</sup> The second method involves the analysis of the electrochemical mechanism via identified model parameters.<sup>[26–29]</sup> Using this approach, the capacity-fading mechanism of lithium-ion cell consisting of  $\text{LiNi}_{x}\text{Co}_{1-x}\text{O}_2$  cathode and a graphite-based anode was determined based on the changes in the model parameters (the initial SOCs of the cathode and anode, and the volume fraction of the cathode) of a single-particle physics-based model.<sup>[27]</sup> In addition, the effect of discharge current density on the degradation mechanism of a generic lithium-ion battery was studied based on the changes in model parameters (the initial SOCs for the positive and the negative electrode and the volume fraction of the positive electrode) of a physics-based pseudo-2D lithium-ion battery model.<sup>[28]</sup> Hence, capacity fade analysis based on the changes in model parameters can be an effective non-destructive method to study the effect of different cell designs and operating conditions on the performance of lithium-ion batteries.

In this study, we adopted the porous composite-electrode physics-based model originally developed by Newman and Tiedman<sup>[30]</sup> and further enhanced by M. Doyle<sup>[31]</sup> to analyze the cycle performance of silicon-based anode half-cells with bare and PD-treated copper current collectors via a parameter estimation technique. Based on the estimation of the parameters that change with cycling, the various mechanisms associated with the capacity fade in the bare and PD-treated copper current collector were investigated. A quantitative analysis of the aging mechanism of silicon-based anodes in terms of Li ions loss is performed and discussed for the two cell configurations. The percentage contribution of the various identified mechanisms were estimated for the cells with the bare and PD-treated copper current collector. By extrapolating the parameters that changed with cycling, the maximum number of cycles required for the complete deterioration of the limiting cell configuration in terms of cycle performance were determined.

## 2. Results and Discussion

### 2.1. Parameter Estimation

The parameters that change with cycling were estimated by fitting the physics-based porous composite electrode model predictions of the voltage profile to those of experimental data obtained from 2032 coin-type cells consisting of silicon electrodes prepared with bare and polydopamine-treated (PD-treated) Cu current collectors at some selected number of cycles. The

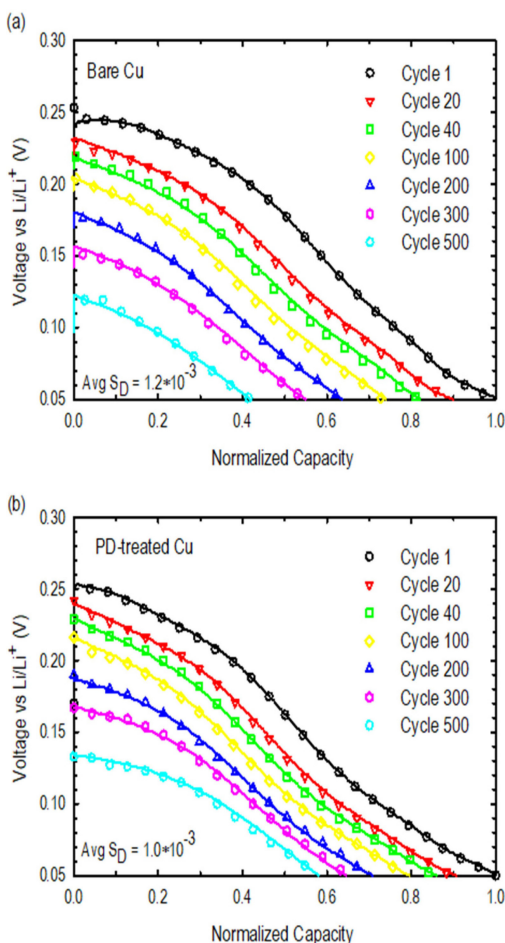


**Figure 1.** Comparison of experimental discharge profiles and physics-based porous composite electrode model predictions for Si/Li half-cells with a) bare Cu current collector and b) polydopamine (PD)-treated Cu current collector. The symbols and the solid lines represent the experimental data and model predictions, respectively.

fitting were done using a nonlinear least square regression technique, the Levenberg Marquardt method. A similar approach was used by S. Santhanagopalan<sup>[32]</sup> to estimate unknown parameters by fitting the single particle and porous electrode model to experimental charge discharge curves of a lithium-ion cell. The results of the fitting are shown in Figure 1. The symbol and the solid lines represent the experimental data and model predictions, respectively. The model predictions were executed using the parameters in Table 1. There is a high correlation between the model predictions and the experimental voltage profiles as confirmed by the lower values of the estimated average standard deviation shown in Figure 1.

To achieve the high correlation between the physics-based model predictions and the experimental voltage profiles of the two cell configurations considered in this study, an optimization technique, which employs the non-linear least square method, was used to estimate the parameters that changed with cycling. For the cells with the bare Cu current collector, three parameters changed with cycling. These parameters are the total film resistance ( $R_{\text{film}}$ ), the initial state of charge ( $x_{0,\text{Si}}$ ) of the silicon electrode, and the maximum Li ion concentration in

**Table 1.** Model parameters used in this study.

Symbol	Parameters	Value
$L_p$	Si electrode thickness, $\mu\text{m}^{\text{a}}$	$8 \times 10^{-6}$
$L_n$	Li metal electrode thickness, $\mu\text{m}^{\text{a}}$	$450 \times 10^{-6}$
$L_s$	Separator thickness, $\mu\text{m}^{\text{a}}$	$20 \times 10^{-6}$
$r$	Si particle radius, $\text{m}^{\text{a}}$	$30 \times 10^{-9}$
$\varepsilon_e$	Volume fraction electrolyte <sup>a</sup>	0.85
$D_{s,p}$	Diffusion coefficient constant of Li in $\text{Li}_x\text{Si}$ , $\text{m}^2\text{s}^{-1}\text{d}^{\text{d}}$	$3 \times 10^{-16}$
$D$	Diffusion coefficient constant of Li in electrolyte, $\text{m}^2\text{s}^{-1}\text{c}^{\text{c}}$	$3.93 \times 10^{-10}$
$k_n$	Reaction rate constant on Li metal, $\text{mol}^{0.5}\text{m}^{-0.5}\text{s}^{\text{c}}$	$6.1 \times 10^{-6}$
$K_1$	Electronic conductivity of Si electrode, $\text{Sm}^{-1}\text{d}^{\text{d}}$	33
$k_p$	Reaction rate constant on Si electrode, $\text{m}^{2.5}\text{mol}^{-0.5}\text{s}^{-1}\text{b}^{\text{b}}$	$2 \times 10^{-12}$
$c_{smax}$	Maximum Li concentration, $\text{mol m}^{-3}\text{d}$	$3.11 \times 10^5$
$\alpha_c$	Cathodic apparent transfer coefficient <sup>b</sup>	0.26
$\alpha_a$	Anodic apparent transfer coefficient <sup>b</sup>	0.74
$R_{film}$	Film resistance, $\Omega\text{m}^2\text{d}^{\text{d}}$	$4.7 \times 10^{-4}$
A	Geometric area of Si electrode, $\text{m}^2\text{a}$	$1.131 \times 10^{-4}$

[a] Parameter set in the cell design [b] Fitted parameter. [c] Obtained from COMSOL library. [d] Parameters based on literature<sup>[32]</sup>

silicon electrode ( $c_{\text{max},\text{Si}}$ ). On the other hand, in addition to the three parameters that changed with cycling for the cells with the bare Cu current collector, the reaction rate constant ( $k_{\text{Si}}$ ) varied with cycling for the cells with the PD-treated Cu current collector. The variations in the parameters with cycling for the two cell configurations are shown in Figure 2. The total resistance increased monotonically with cycling and was higher in the cells with the bare Cu current collector compared to the cells with PD-treated Cu current collector (Figure 2a). The film resistance is the sum of the resistance due to the SEI and that due to the contact between the silicon composite material and the Cu current collector. Moreover, the initial SOC of the silicon electrode ( $x_{0,\text{Si}}$ ) increased with cycling for the two cell configurations (Figure 2b). The rate of increase was high during the initial stages of the cycling but reduces as the cycling proceeds and eventually becomes almost constant at the later part of cycling. The rate of increase was higher for the cells with bare Cu current collector relative to the cells with PD-treated Cu current collector. Figure 2b indicates that the silicon electrode becomes less discharged with cycling. The maximum Li ion concentration of silicon for the two cell configurations also increased with cycling and it was higher for the cells with bare compared to the cells with the PD-treated Cu current collector (Figure 2c). The increase in the maximum Li ion concentration can be attributed to the additional supply of Li ions from the reference Li metal electrode as cycling progressed. Lastly, the reaction rate constant also decreased with cycling for the cell with the PD-treated Cu current collector but remains constant for the cells with the bare Cu collector (Figure 3d). This was due to the insulating nature of the polydopamine interlayer and a detailed discussion will be given in the subsequent section. The changes in the film resistance (contact) reflects the mechanical degradation while that in the

initial SOC reflects both chemical (SEI formation) and mechanical degradation (Li ions loss due to particle isolation).

The predicted SOCs of the silicon electrode at the end-of-charge (EOC) for the cells with bare and PD-treated Cu current collectors is shown in Figure 3. At EOC, the silicon electrode in both cell configurations becomes less charged ( $x_{\text{Si}}$  decreases). The rate at which the SOC at EOC decreased was high during the initial cycles (1 to 40) but reduced at midway (40 to 400) through the cycling and became lesser at the later part of cycling (400 to 500). The polydopamine interlayer did not have any significant effect on the rate at which the silicon electrode became less lithiated at the end of the 500 cycles.

## 2.2. Model Predictions

To conduct further analysis beyond the 500 cycles, we tried to predict the cycle performance of the cells with bare and the PD-treated Cu current collectors at higher number of cycles by extrapolating the model parameters that change with cycle number to 1000 cycles. The parameter extrapolation was done based on the assumption that the capacity-fading mechanism remained the same during the period of the predictions. The extrapolated model parameters are presented in Figure 4.

The extrapolated model parameters in Figure 4 were used to predict the cycle performance of the cells with bare and PD-treated Cu current collectors. The outcome of the predictions are shown in Figure 5. A comparison between the experimental normalized charge capacity retention and the model predictions during the first 500 cycles for the two cell configurations are presented in Figure 5. There was a good match between the experimental data and model predictions. In addition, a prediction of the normalized charge capacities using an empirical model (Table 2) is shown in Figure 5. A stage of accelerated capacity deterioration is predicted after ca. 690 cycles for the cells with the bare Cu current collector (Figure 5a). This is in agreement with previously published experimental results by Mazouzi et al.,<sup>[33]</sup> where they observed a drastic capacity decay for Si/Li half-cell after 700 cycles. A continuous accelerated capacity decay is predicted for the cells with PD-treated Cu current collector. The shape of the capacity fade pattern predicted in Figure 5b is similar to that observed experimentally by Song et al.<sup>[34]</sup>

Figure 6 shows the simulated silicon electrode SOC at the EOC for cells with bare and PD-treated Cu current collectors using the extrapolated model parameters in Figure 4. The SOC at EOC decrease steadily for both cell configurations. The prediction did not show any significant changes in the SOC at EOC for the extended number of cycles. Thus, the capacity-mechanisms remained the same as that predicted during the

**Table 2.** Empirical model expressions and parameters.

Cell Design	Model	A	B	C	D
Bare Cu	$Ax^B + Cx + D$	-0.1659	0.1973	-0.0004228	1.193
PD-treated Cu	$Ax^B + Cx + D$	-0.0299	0.4861	0.0003641	1.026

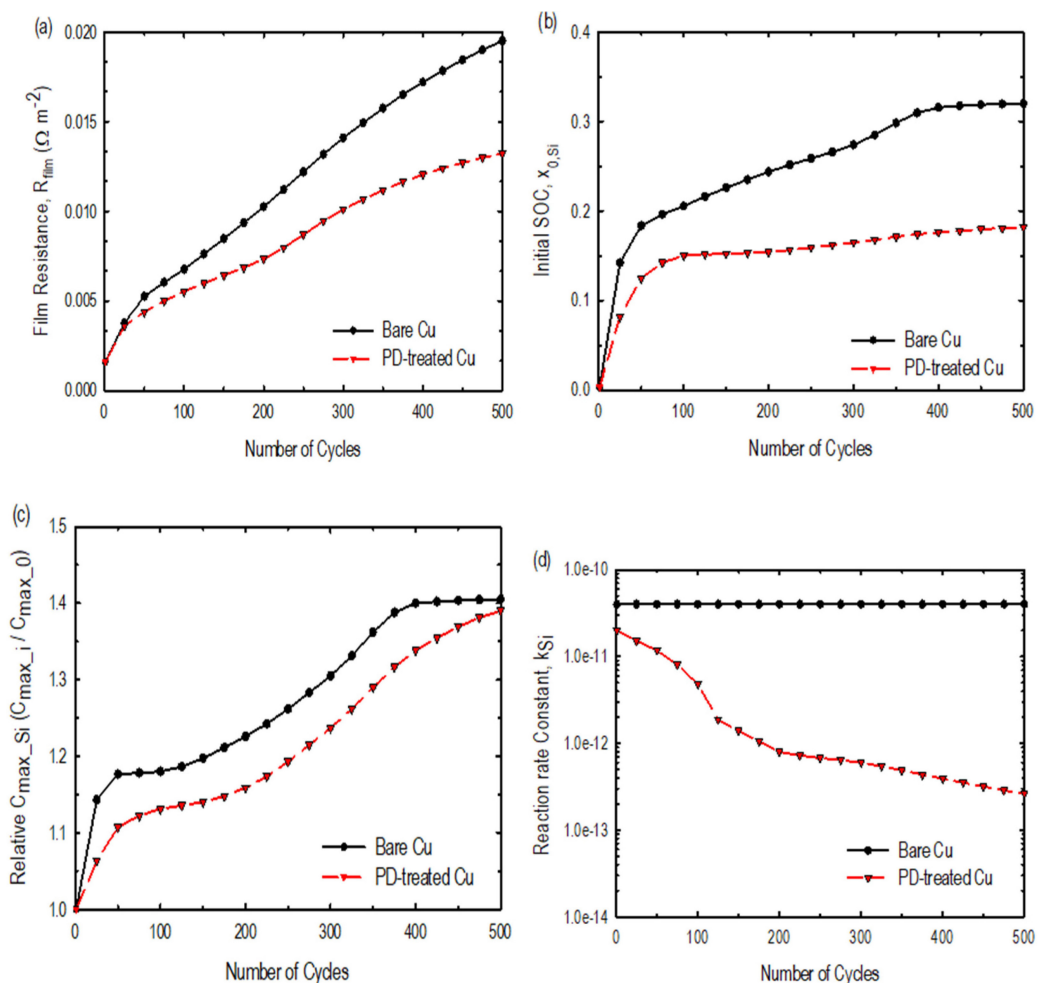


**Figure 2.** The changes of model parameters with cycling (obtained from fitting the experimental voltage profiles for each cycle).

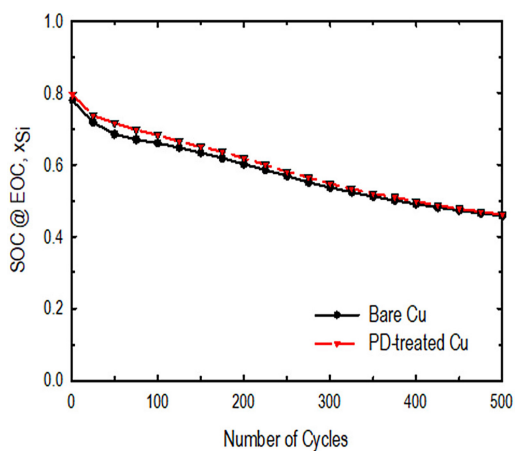


**Figure 3.** The simulated SOCs for the Si/Li half-cells with bare and polydopamine (PD)-treated Cu current collectors at the end of charge (EOC) predicted by the physics-based porous composite electrode model using the parameters presented in Figure 2.

initial 500 cycles. The capacity fade of the two cell configurations will be analysed using the information obtained from the physics-based model.

### 2.3. Capacity Fade Analysis

The results presented in the previous sections suggests that, the presence of the PD interlayer between the silicon composite electrode and the Cu current collector has a significant positive effect on the capacity fade of Li/Si half-cells. In this section, we try to discuss the phenomenon constituting these effects.

The study performed on the parameters that change with cycling shows that, the film resistance increases with cycling for both cell configurations with the rate of increase being higher in the cells with bare Cu current collector (see Figure 2). Here, the film resistance is the sum of the resistance due to the formation of the SEI and the contact resistance between the silicon composite electrode and the Cu current collector. However, since the cells with both bare and PD-treated Cu, current collectors have silicon as their anode active material; there will be no significance difference between the increases in resistance due to the formation of SEI. Thus, the main difference between the film resistance of the bare and PD-treated Cu current collector can be attributed to the different contact resistances between the silicon composite electrode and the Cu current collector. Cho et al.<sup>[6]</sup> have demonstrated

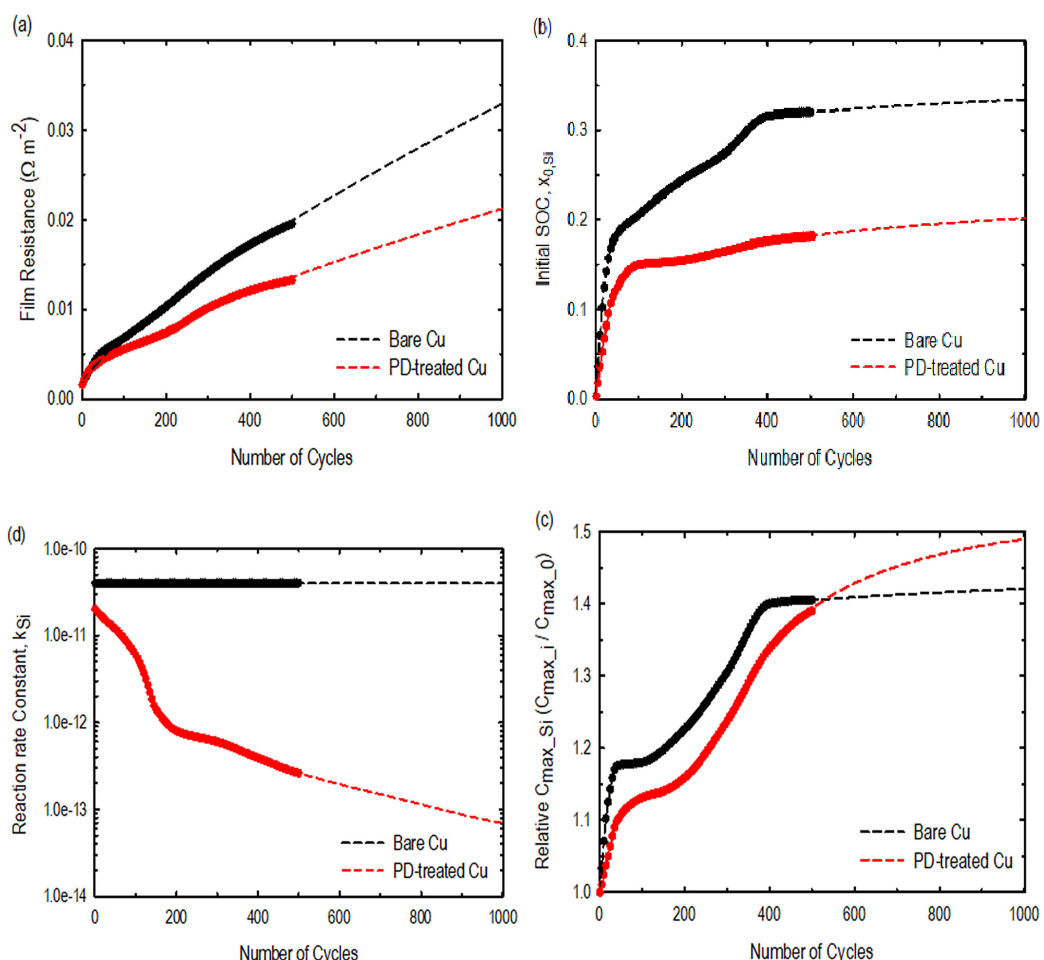


**Figure 4.** The extrapolation of the physics-based porous composite electrode model parameters that changed with cycling in Figure 2. The extrapolations were obtained using the curve-fitting tool in Matlab.

this experimentally, where they attributed the improvement in the cycle performance of the cells with PD-treated Cu current collector, to the enhanced adhesion strength between the silicon composite electrode and Cu current collector. The increase in the adhesion strength resulted in a lower contact resistance as demonstrated in Figure 2.

In addition, many previous reports have been made on the occurrence of side reactions on silicon electrodes during (de) lithiation processes.<sup>[20,35–37]</sup> These side reactions are known to consume Li ions resulting in the formation of the SEI on the surface of the silicon electrode. Two types of SEI have been reported to form during the (de) lithiation processes.<sup>[38]</sup> First is the formation of diethyl 2,5-dioxahexane dicarboxylate (DEDOHC) during the early stage of cycling when 1 M LiPF<sub>6</sub>/EC:DEC (1:2 v/v) electrolyte is used. The DEDOHC is known to be non-conductive and increases the impedance of the cell. The co-product of the formation of DEDOHC, Li propionate also traps Li ions contributing to low columbic efficiency of the cell. In this work, we used 1.15 M LiPF<sub>6</sub>/EC:EMC (3:7 v/v) electrolyte. Hence the SEI product formed, assuming that the formation mechanism is similar to that of DEDOHC, will be ethyl methyl 2,5-dioxahexane dicarboxylate (EMDOHC) which is assumed to have similar properties as the DEDOHC. Second is the formation

of lithium ethylene dicarbonate (LiEDC), when lithiated silicon is exposed to the electrolyte because of crack formation owing to volume expansion in silicon electrodes. The formation of the two types of SEI leads to the loss of cyclable Li ions. The mechanism for the formation of the EMDOHC and LiEDC can be described as, Scheme 1.

In addition, the volume expansion in silicon electrodes causes the physical or electrochemical isolation of active materials from the conduction pathway, dead silicon that cannot contribute to capacities. The dead silicon also traps cyclable Li ions leading to capacity fade.<sup>[2,10,39]</sup>

We address the capacity loss to the formation of the SEI and dead silicon particles for the Si/Li half-cells with bare and PD-treated Cu current collectors in terms of percentage of Li ions loss to the capacity fade. To do this, we considered two main cases. In the first case, we assume that, there is no supply of excess Li ions from the Li metal, thus the capacity retention depends on the initial capacity of the cell after the first cycle. During the first cycle, the silicon electrode is charged from Li<sub>(0.01)</sub>Si to Li<sub>(2.6)</sub>Si ( $x_{\text{Si}} = 0.003$ ,  $x_{\text{Si}} = 0.78$  in Figure 2b and Figure 3 respectively). After 40 cycles the silicon electrode is lithiated from Li<sub>(0.59)</sub>Si to Li<sub>(2.31)</sub>Si ( $x_{\text{Si}} = 0.18$ ,  $x_{\text{Si}} = 0.69$  in Figure 2b and Figure 3, respectively). The fraction of the total Li

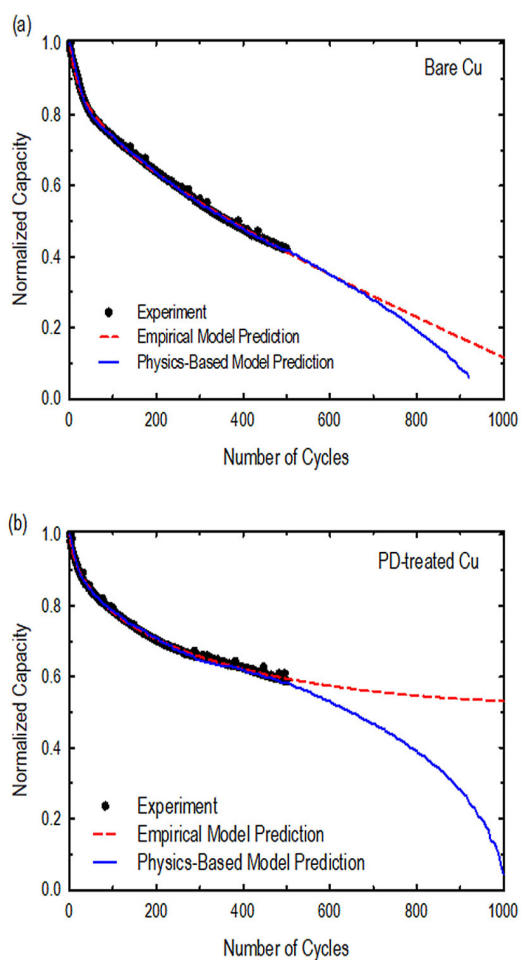


**Figure 5.** Comparison of the normalized charge capacity as a function of number of cycles predicted by the physics-based porous composite electrode model and empirical model for the Si/Li half-cells with a) bare and b) PD-treated Cu current collectors. The physics-based model predicted a fast decay of the normalized capacity in both cell configurations.

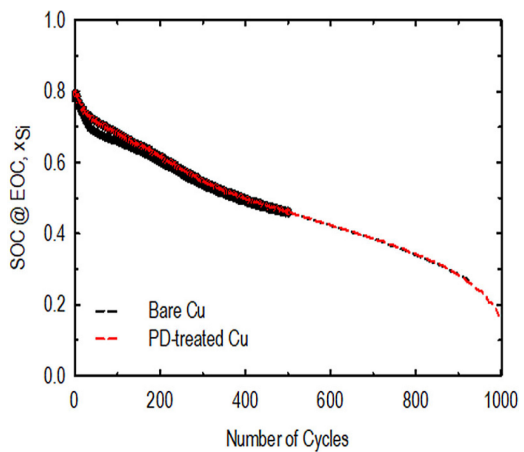
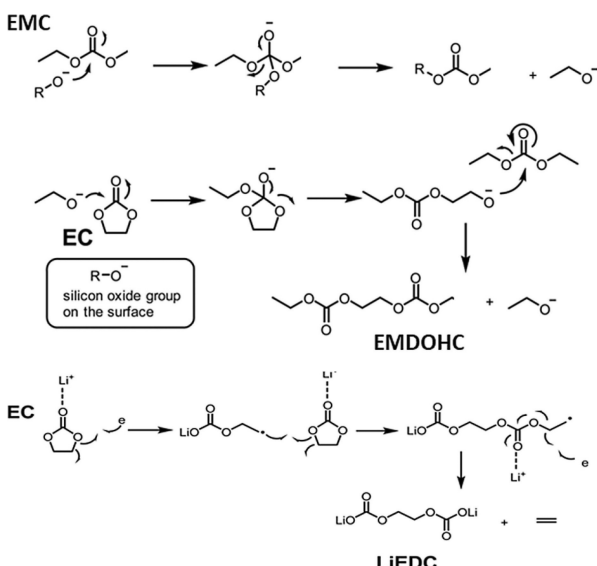


**Figure 6.** The predicted SOCs for the bare and PD-treated Cu current collectors at the EOC using the extrapolated physics-based porous composite electrode model parameters presented in Figure 4. The symbols show the SOC at EOC in Figure 3.



**Scheme 1.** The formation mechanism of EMDOHC and LiEDC.

ions loss after the 40th cycle is  $(2.6 - (2.31 - (0.59 - 0.01))) / (2.6 - 0.01) = 0.34$  for the cells with bare Cu current collector. The capacity loss of the cell in terms of Li ions trapped in the isolated silicon is  $(0.59 - 0.01) / (2.6 - 0.01) = 0.22$ . The remaining fraction of Li ions loss is to the formation of the SEI. Similar calculations were done for the cells with the PD-treated Cu current collector and the results are displayed in Figure 7a and 7b. The rate of SEI formation on just produced lithium-ion cells are very high and it is known to control the capacity fade during pre-cycling.<sup>[40]</sup> However, we conducted the capacity-fading analysis after the pre-cycling stage. Hence, from Figure 7a, the capacity fading due to the loss of Li ions in cells with the bare Cu current collector is controlled by the Li ions trapped in the isolated silicon during cycling but becomes almost the same at the end of the 500 cycles. In Figure 7b, the capacity fading due to loss of Li ions in the cells with PD-treated Cu current collector is dominated by the Li ions trapped in isolated silicon during the initial stages of cycling, but it was overtaken by the Li ions loss to the SEI formation after 150 cycles. The loss of Li ions to SEI formation was similar for the two cell configurations as shown in Figure 7. The only difference was in the loss of Li ions to the isolation of the silicon active material and was higher in the cells with bare Cu current collector. Thus, the presence of the PD interlayer between the silicon composite electrode and Cu current collector aids in the reduction in the formation of dead silicon and hence improves the capacity of the cell.

In the second case, we considered the effect of the additional Li ions from the Li metal and presented the results of the net loss of Li ions as function of number of cycles for the bare and PD-treated Cu current collectors in Figure 7c and 7d, respectively. From the model parameters that change with cycling in Figure 2, the maximum Li ion concentration ( $c_{\max, \text{Si}}$ ) was found to increase with cycling (Figure 2c). The increase in  $c_{\max, \text{Si}}$  is due to the additional supply of Li ions from the Li metal after the first cycle. Similar to the estimation of Li ion loss in the

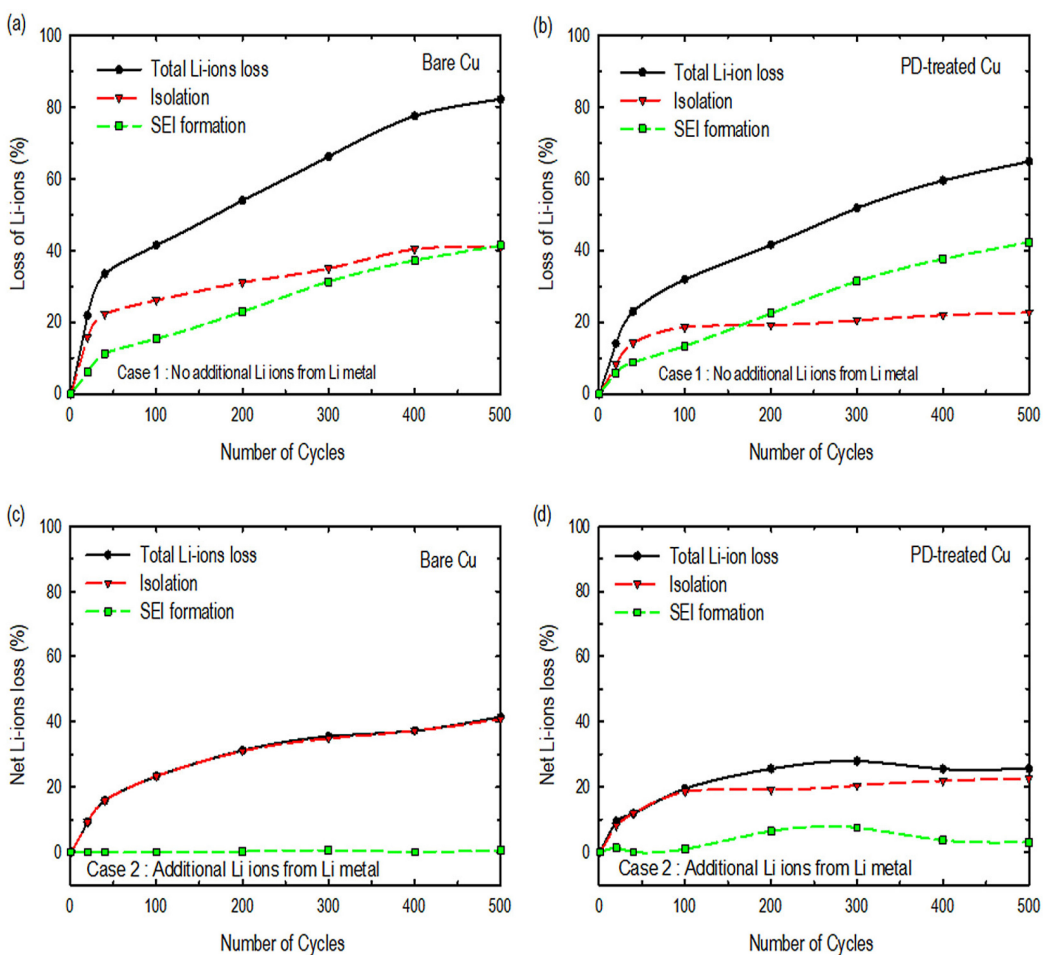
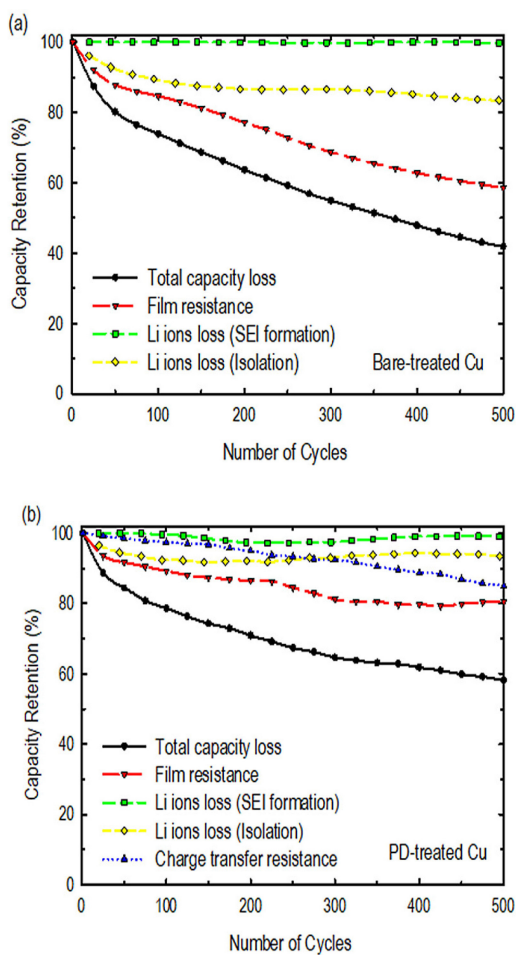


**Figure 7.** The percentage of Li ion loss in Si/Li half-cells with a) bare Cu current collector and b) PD-treated Cu current collector, estimated based on the assumption that, no additional Li ions are supplied from the Li metal. The net loss of Li ions in Si/Li half-cells with c) bare Cu current collector and d) PD-treated Cu current collector, estimated considering the effect of the excess Li ions from the Li metal.

first case, the silicon electrode was charged from  $\text{Li}_{(0.01)}\text{Si}$  to  $\text{Li}_{(2.6)}\text{Si}$ . However, during the 40th cycle, the silicon electrode was charged from  $\text{Li}_{(0.59)}\text{Si}$  to  $\text{Li}_{(3.05)}\text{Si}$  ( $x_{\text{Li},\text{Si}} = 0.003$ ,  $x_{\text{Si}} = 0.92$  ( $x_{\text{Si}} = x_{\text{Si}}^0 \times (c_{\text{max},j} / c_{\text{max},0})$ , where  $x_{\text{Si}}^0$  is the SOC at EOC during the first cycle). There was a 0.74 increase in the stoichiometric content of Li ions in the charged state relative to when the effect of Li metal was not considered. Thus, the fraction of total Li ions loss after the 40th cycle is reduced from 0.34 to 0.17. This excess Li ion is assumed to replenish the Li ion loss to the SEI formation. This assumption was made based on the fact that, the amount of Li ions trapped in the film formation cannot account for the cumulative capacity retention of the cells due to the unlimited supply of Li ions from the Li metal as demonstrated experimentally by Delpuech et al.<sup>[36]</sup> by using quantitative Li NMR<sup>[21]</sup> spectroscopy. On the other hand, the Li ions trapped in the isolated silicon particles contributes to the cumulative capacity retention due to the reduction in the holding capacity of the silicon electrode. The net loss of Li ions to SEI formation in the cells with the bare Cu current collector is ca 0% at the 500 cycle (Figure 7c) while that in the cells with the PD-treated is ca. 4%. This is because the amount of the silicon particles in the cells with PD-treated Cu current collector

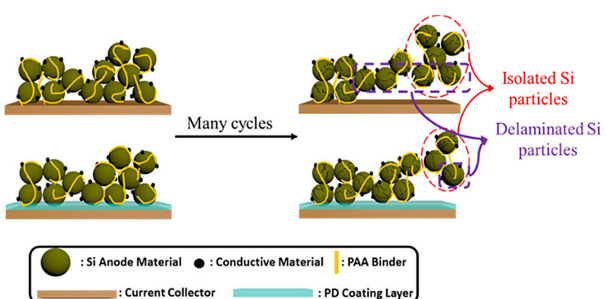
after the 500 cycles is quite higher and most of them are exposed to the electrolyte after lithiation leading to high LiEDC formation. Thus, the excess Li ions supplied from the Li metal were not enough to replenish those losses to the SEI formation.

Figure 8 shows the percentage contribution of the film resistance (SEI resistance and contact resistance), Li ion loss to SEI formation and Li ions trapped in the isolated silicon particles towards the reduction of the capacity retention of the cells with the bare and PD-treated Cu current collector corresponding to the result in Figure 1. The calculations of the percentage contribution of the Li ion losses were done based on the assumption used in the second case in Figure 7. The film resistance contribute to ca. 41.4 and 19.51% in the capacity reduction in the cells with bare and PD-treated Cu current collectors, respectively. Thus, the presence of the PD-interlayer reduces the effect of the film resistance (contact resistance) by ca. 22% at the end of 500 cycles. This reduction in the contact resistance can be attributed to the increase in adhesion strength<sup>[15]</sup> owing to the ability of the polydopamine interlayer to form covalent bonds<sup>[41]</sup> with polyacrylic acid binder in the silicon composite. The loss of the capacity to isolation of the silicon active material contributed to 16.6 and 6.5% in the bare



**Figure 8.** Relative contribution of the film resistance (SEI resistance and contact resistance), Li ions loss to SEI formation and Li ions trapped in the isolated silicon active material to the total capacity fade corresponding to the results in Figure 1 in Si/Li half-cells with a) bare Cu current collector and b) PD-treated Cu current collector.

and PD-treated Cu current collectors, respectively. Thus, the polydopamine interlayer also reduces the capacity loss to the isolation of the silicon particles by ca. 10%. Owing to the strong adhesion between the silicon composite electrode and the Cu



**Scheme 2.** The effect of the polydopamine interlayer on the number of isolated particles after several cycles. Less number of Si particles are isolated due to the stronger attraction force exerted on the Si particles at the surface of the electrode by those in contact with the Cu current collector.

current collector by the PD interlayer, the silicon particles at the surface of the electrode prone to isolation experiences a higher force of attraction as compared to those in the cells with the bare Cu current collector. A schematic representation of this phenomenon is presented in Scheme 2. Since the amount of Li ion loss to the formation of the SEI cannot account for the capacity retention due to the unlimited supply of Li ions from the Li metal, its percentage contribution was almost negligible with a value less than 1% in the two cell configurations. The reduction in the reaction rate constant in Figure 2d can be attributed to the continuous passivation of the surface of the electrode by an insulating film during cycling.<sup>[42]</sup> The reduction in the electrochemical rate constant result in a slow charge transfer process at the electrode/electrolyte interface (reduction in the  $j_p$  in the PCE model (Table 3)). This results in an increase in the charge transfer resistance, which contributes to a ca. 15% reduction in the capacity retention.

### 3. Conclusions

The effect of polydopamine interlayer between silicon composite electrode and Cu current collector on the cycle performance of silicon-based anode was analyzed by fitting the predictions of a physics-based porous composite electrode model to experimental discharge curves obtained from cycling

**Table 3.** An overview of the governing equations and boundaries conditions used in the Porous Composite Electrode (PCE) framework.

Cell compartment	Name	Governing equations
Li metal	Butler-Volmer equation	$j_n = k_n (c_{n,max} - c_{n,surf})^{0.5} c_{n,surf}^{0.5} \times [\exp(\frac{0.5F}{RT} \eta_n) - \exp(-\frac{0.5F}{RT} \eta_n)]$
Separator	Over-potential	$\eta_n = \phi_1 - \phi_2 - U_n$
	Material, liquid phase	$\epsilon \frac{\partial c_e}{\partial t} = \frac{\partial}{\partial x} (D_{eff,s} \frac{\partial c_e}{\partial x})$
Cathode	Charge, liquid phase	$-\kappa_{eff,s} \frac{\partial \phi_{2,s}}{\partial x} + \frac{2RT(1-t^0)}{F} \kappa_{eff,s} \frac{\partial \ln c_e}{\partial x} = 0$
	Material, solid phase	$\frac{\partial c_{e,p}}{\partial t} = D_{s,p} \frac{1}{t^2} \frac{\partial}{\partial r} (r^2 \frac{\partial c_{e,p}}{\partial r})$
	Charge, solid phase	$\sigma_{s,eff}^{eff} \frac{\partial^2 \phi_{1,p}}{\partial x^2} = a_{s,p} F j_p$
	Material, liquid phase	$\epsilon_{e,p} \frac{\partial c_{e,p}}{\partial x} = \frac{\partial}{\partial x} (D_{eff,p} \frac{\partial c_{e,p}}{\partial x}) + (1-t^0) a_{s,p} j_p$
	Charge, liquid phase	$- \frac{\partial}{\partial x} (\kappa_{eff,p} \frac{\partial \phi_{2,p}}{\partial x}) + \frac{2RT(1-t^0)}{F} \frac{\partial}{\partial x} (\kappa_{eff,p} \frac{\partial \ln c_e}{\partial x}) = a_{s,p} F_p$
	Butler-Volmer equation	$j_p = \kappa_p (c_{p,max} - c_{p,surf})^{0.5} c_{p,surf}^{0.5} c_{e,p}^{0.5} \times [\exp(\frac{0.5F}{RT} \eta_p) - \exp(-\frac{0.5F}{RT} \eta_p)]$
	Over-potential	$\eta_p = \phi_1 - \phi_2 - U_p - R_{film} j_i$

Si/Li half-cells with bare and PD-treated Cu current collectors. By examining the model parameters that change with cycling, the various capacity-fading mechanisms in the Si/Li half-cells with bare and PD-treated Cu current collector were established and discussed. Based on our analysis, the major capacity-fading mechanisms in Si/Li half-cells are the increase in the film resistance (SEI resistance and contact resistance) and the isolation of silicon active materials. The presence of the polydopamine interlayer resulted in the reduction in the capacity loss to the film resistance (contact resistance) and the Li ions trapped in the isolated silicon active material by ca. 22 and 10%, respectively. The Li ion loss to the formation of the SEI did not have any profound effect on the capacity retention owing to the unlimited supply of Li ions from the Li metal in the half-cell. The insulating-nature of the polydopamine interlayer lead to a reduction in the reaction rate constant resulting in an increase in the charge transfer resistance. This contributed to ca. 15% reduction in the capacity retention. Thus for a further improvement in the cycle performance of the silicon-based anode, a more conductive interlayer between the silicon composite material and the copper current collector should be employed.

## Experimental Section

### Treatment of Cu Current Collector with Polydopamine

The coating process described by Ryou et al.<sup>[43]</sup> was adopted to coat the polydopamine (PD) on the Cu current collector. The mixture used to make the dopamine solution ( $2 \text{ mg mL}^{-1}$ ) contained Tris buffer solution (pH 8.5, 10 mM) and methanol ( $\text{CH}_3\text{OH}/\text{buffer} = 1/1 \text{ wt\%}$ ).

### Preparation of Electrode

The composition of the slurry used to make the Si electrode was 60 wt% Si active material (30 nm; Nanostructured & Amorphous Materials, Inc, Houston, USA), 20 wt% conductive material (Super-P, Timcal, Switzerland) and 20 wt% poly (acrylic acid) (MW = 450,000; Sigma-Aldrich, South Korea) binder in deionized water. The prepared slurry was cast onto the bare current collector (8  $\mu\text{m}$ ; IJIN Materials, South Korea) and PD-treated Cu current collector using a doctor blade and dried in a convection oven at  $80^\circ\text{C}$  for 2 h. The loading level and thickness of the Si electrode were controlled to  $0.53 \text{ mg cm}^{-2}$  and 8  $\mu\text{m}$  respectively.

### Assembling of Cell

2032 coin half-cells were fabricated with the prepared Si electrodes (diameter: 12 mm; dried in a vacuum oven at  $60^\circ\text{C}$  for 12 h before use), Li metal (450  $\mu\text{m}$ ; Honjo Metal Co., Japan) as the counter electrode, and a polyethylene separator ((ND420, Asahi Kasei, Japan). The porous part of the separator was filled with a liquid electrolyte (1.15 M LiPF<sub>6</sub> in ethylene carbonate/ethyl methyl carbonate; EC/EMC = 3/7 vol%; Panax Etec, South Korea). The electrolyte contained 5 wt% fluoroethylene carbonate (Panax Etec, South Korea). The coin cells were assembled in an argon-filled glove box with constant dew point less  $-80^\circ\text{C}$ .

### Measurement of Electrochemical Performance

The assembled coin cells made of were aged for 12 h prior to the evaluation of the formation step and cycle performance using a battery tester (PNE Solution, South Korea). The cells were cycled between 0.05 and 2.0 V at a constant current density of  $0.2 \text{ A g}^{-1}$  at room temperature during the formation step. The cells were then cycled at a constant current density of  $1.2 \text{ A g}^{-1}$  for 500 cycles.

### Mathematical Model

Newman and Tiedemann<sup>[30]</sup> originally developed the physics-based porous composite electrode (PCE) model adapted in this study to simulate the silicon composite electrode. The PCE model after its development was upgraded<sup>[31,44]</sup> and used by other researchers for simulating various chemistries of Li ion battery.<sup>[16,45–47]</sup>

The PCE model addresses the relations of the above system with a specific geometrical, material and functional approximations. The model treats the working electrode and the reference electrode as independent homogenized continuum with effective properties as dictated by the Bruggeman's relationship. In general, the PCE model considers the material balance on the solid-phase material balance on the electrolyte (which assumes that all the reaction involves Li ion), Ohm's law in the solid-phase and liquid-phases. The intrinsic characteristic of the electrochemical reaction that takes place at the surface of the silicon composite electrode particles and the Li metal are modelled separately by the Butler-Volmer equation. The PCE unlike other physics-based model such as the single particle model, accounts for the diffusion phase limitations, which makes it suitable for this study. The set of equations used in the PCE were solved using COMSOL Multiphysics 5.2 and their boundary conditions are given in Table 3.

### Nomenclature

$a_{s,i}$	specific surface area of electrode $i$ ( $i=p, n$ ), $\text{m}^{-1}$
$c_e$	concentration of electrolyte, $\text{mol m}^{-3}$
$c_{s,i}$	concentration of lithium-ions in the solid phase of electrode $i$ ( $i=p, n$ ), $\text{mol m}^{-3}$
$c_{s,i,\text{ini}}$	initial concentration of lithium-ions in the solid phase of electrode $i$ ( $i=p, n$ ), $\text{mol m}^{-3}$
$c_{s,i,\text{max}}$	maximum concentration of lithium-ions in the solid phase of electrode $i$ ( $i=p, n$ ), $\text{mol m}^{-3}$
$D$	electrolyte diffusion coefficient, $\text{m}^2 \text{s}^{-1}$
$D_{s,i}$	lithium-ion diffusion coefficient in the solid phase of electrode $i$ ( $i=p, n$ ), $\text{mol m}^{-3}$
$F$	Faraday's constant, $96487 \text{ C mol}^{-1}$
$j$	pore wall flux of lithium-ions, $\text{mol m}^{-2} \text{s}^{-1}$
$k_i$	intercalation/deintercalation reaction rate constant of electrode $i$ ( $i=p, n$ ), $\text{m}^{-2.5} \text{ mol}^{-0.5} \text{s}^{-1}$
$L_n$	thickness of negative electrode, $\text{m}$
$L_s$	thickness of separator, $\text{m}$
$L_p$	thickness of positive electrode, $\text{m}$
$r$	radial coordinate, $\text{m}$
$R_i$	radius of active material of electrode $i$ ( $i=p, n$ ), $\text{m}$
$R_{SEI}$	film resistance at the electrode/electrolyte interface, $\Omega \text{m}^2$
$t_+$	cation transference number
$T$	ambient temperature, $\text{K}$
$U_0$	equilibrium potential, $\text{V}$
$\varepsilon$	volume fraction

$\eta$	local over potential, V
$\kappa$	ionic conductivity of the electrolyte, Sm <sup>-1</sup>
$\sigma_i$	electronic conductivity of the solid phase of electrode <i>i</i> ( <i>i</i> =p, n), Sm <sup>-1</sup>
$\phi_1$	solid phase electric potential, V
$\phi_2$	solution phase electric potential, V

## Acknowledgements

This work was supported by Technology Development Program (S2414576) funded by the Ministry of SMEs and Startups (MSS, Korea). This research was also supported by Korea Electric Power Corporation (Grant number: R17XA05-79). We also appreciated the support from the DGIST Supercomputing and Bigdata Center.

## Conflict of Interest

The authors declare no conflict of interest.

**Keywords:** Lithium-ion batteries • Adhesion property • Silicon electrode • Polydopamine interlayer • Capacity fade analysis

- [1] W.-J. Zhang, *J. Power Sources* **2011**, *196*, 13–24.
- [2] H. Wu, Y. Cui, *Nano Today* **2012**, *7*, 414–429.
- [3] C.-M. Park, J.-H. Kim, H. Kim, H.-J. Sohn, *Chem. Soc. Rev.* **2010**, *39*, 3115–3141.
- [4] M. M. Thackeray, C. Wolverton, E. D. Isaacs, *Energy Environ. Sci.* **2012**, *5*, 7854–7863.
- [5] M. Ko, S. Chae, J. Ma, N. Kim, H.-W. Lee, Y. Cui, J. Cho, *Nat. Energy* **2016**, *1*, 16113.
- [6] M. T. McDowell, S. W. Lee, W. D. Nix, Y. Cui, *Adv. Mater.* **2013**, *25*, 4966–4985.
- [7] C. K. Chan, H. Peng, G. Liu, K. McIlwrath, X. F. Zhang, R. A. Huggins, Y. Cui, *Nat. Nanotechnol.* **2008**, *3*, 31–35.
- [8] J. S. Bridel, T. Azais, M. Morcrette, J. M. Tarascon, D. Larcher, *J. Electrochem. Soc.* **2011**, *158*, A750–A759.
- [9] J. B. Bates, N. J. Dudney, B. Neudecker, A. Ueda, C. D. Evans, *Solid State Ionics* **2000**, *135*, 33–45.
- [10] Y. Son, J. Sung, Y. Son, J. Cho, *Curr. Opin. Electrochem.* **2017**, *6*, 77–83.
- [11] J. Choi, K. Kim, J. Jeong, K. Y. Cho, M.-H. Ryou, Y. M. Lee, *ACS Appl. Mater. Interfaces* **2015**, *7*, 14851–14858.
- [12] L. Shen, L. Shen, Z. Wang, L. Chen, *ChemSusChem* **2014**, *7*, 1951–1956.
- [13] A. Magasinski, B. Zdyrko, I. Kovalenko, B. Hertzberg, R. Burtovyy, C. F. Huebner, T. F. Fuller, I. Luzinov, G. Yushin, *ACS Appl. Mater. Interfaces* **2010**, *2*, 3004–3010.
- [14] D. Mazouzi, B. Lestriez, L. Roué, D. Guyomard, *Electrochim. Solid-State Lett.* **2009**, *12*, A215–A218.
- [15] I. Cho, S. Gong, D. Song, Y.-G. Lee, M.-H. Ryou, Y. M. Lee, *Sci. Rep.* **2016**, *6*.
- [16] W. A. Appiah, J. Park, S. Byun, I. Cho, A. Mozer, M.-H. Ryou, Y. M. Lee, *J. Power Sources* **2018**, *407*, DOI 10.1016/j.jpowsour.2018.06.079.
- [17] W.-R. Liu, M.-H. Yang, H.-C. Wu, S. M. Chiao, N.-L. Wu, *Electrochim. Solid-State Lett.* **2005**, *8*, A100–A103.
- [18] S. Park, T. Kim, S. M. Oh, *Electrochim. Solid-State Lett.* **2007**, *10*, A142–A145.
- [19] D. Reyter, S. Rousselot, D. Mazouzi, M. Gauthier, P. Moreau, B. Lestriez, D. Guyomard, L. Roué, *J. Power Sources* **2013**, *239*, 308–314.
- [20] C. C. Nguyen, S.-W. Song, *Electrochim. Acta* **2010**, *55*, 3026–3033.
- [21] L. Baggetto, R. A. H. Niessen, P. H. L. Notten, *Electrochim. Acta* **2009**, *54*, 5937–5941.
- [22] M. Dubarry, V. Svoboda, R. Hwu, B. Y. Liaw, *Electrochim. Solid-State Lett.* **2006**, *9*, A454–A457.
- [23] M. Dubarry, C. Truchot, B. Y. Liaw, *J. Power Sources* **2014**, *258*, 408–419.
- [24] M. Dubarry, C. Truchot, B. Y. Liaw, *J. Power Sources* **2012**, *219*, 204–216.
- [25] M. Dubarry, B. Y. Liaw, *J. Power Sources* **2009**, *194*, 541–549.
- [26] L. Zhang, J. Li, C. Lyu, in 2016 IEEE Int. Conf. Progn. Heal. Manag., **2016**, pp. 1–7.
- [27] Q. Zhang, R. E. White, *J. Power Sources* **2008**, *179*, 793–798.
- [28] L. L. Lam, R. B. Darling, *J. Power Sources* **2015**, *276*, 195–202.
- [29] W. A. Appiah, M.-H. Ryou, Y. M. Lee, *J. Electrochem. Soc.* **2019**, *166*, A5109–A5116.
- [30] J. Newman, W. Tiedemann, *AIChE J.* **1975**, *21*, 25–41.
- [31] M. Doyle, T. F. Fuller, J. Newman, *J. Electrochem. Soc.* **1993**, *140*, 1526–1533.
- [32] C. Zhang, S. Santhanagopalan, M. A. Sprague, A. A. Pesaran, *J. Power Sources* **2015**, *290*, 102–113.
- [33] D. Mazouzi, N. Delpuech, Y. Oumellal, M. Gauthier, M. Cerbelaud, J. Gaubicher, N. Dupré, P. Moreau, D. Guyomard, L. Roué, *J. Power Sources* **2012**, *220*, 180–184.
- [34] D. Song, D. Jung, I. Cho, M. Ryou, Y. M. Lee, *Adv. Mater. Interfaces* **2016**, *3*, 1600270.
- [35] M. Winter, *Zeitschrift für Phys. Chemie* **2009**, *223*, 1395–1406.
- [36] N. Delpuech, N. Dupré, P. Moreau, J. Bridel, J. Gaubicher, B. Lestriez, D. Guyomard, *ChemSusChem* **2016**, *9*, 841–848.
- [37] Y. Oumellal, N. Delpuech, D. Mazouzi, N. Dupré, J. Gaubicher, P. Moreau, P. Soudan, B. Lestriez, D. Guyomard, *J. Mater. Chem.* **2011**, *21*, 6201–6208.
- [38] F. Shi, P. N. Ross, G. A. Somorjai, K. Komvopoulos, *J. Phys. Chem. C* **2017**, *121*, 14476–14483.
- [39] N. Dupré, P. Moreau, E. De Vito, L. Quazuguel, M. Boniface, A. Bordes, C. Rudisch, P. Bayle-Guillemaud, D. Guyomard, *Chem. Mater.* **2016**, *28*, 2557–2572.
- [40] M. Nie, D. P. Abraham, Y. Chen, A. Bose, B. L. Lucht, *J. Phys. Chem. C* **2013**, *117*, 13403–13412.
- [41] C.-T. Chen, F. J. Martin-Martinez, G. S. Jung, M. J. Buehler, *Chem. Sci.* **2017**, *8*, 1631–1641.
- [42] R. A. Zangmeister, T. A. Morris, M. J. Tarlov, *Langmuir* **2013**, *29*, 8619–8628.
- [43] M. H. Ryou, Y. M. Lee, J. K. Park, J. W. Choi, *Adv. Mater.* **2011**, *23*, 3066–3070.
- [44] J. H. Waite, *Nat. Mater.* **2008**, *7*, 8–9.
- [45] W. A. Appiah, J. Park, S. Byun, M.-H. Ryou, Y. M. Lee, *J. Electrochem. Soc.* **2016**, *163*, A2757–A2767.
- [46] J. Park, W. A. Appiah, S. Byun, D. Jin, M.-H. Ryou, Y. M. Lee, *J. Power Sources* **2017**, *365*, 257–265.
- [47] A. Jokar, B. Rajabloo, M. Désilets, M. Lacroix, *J. Power Sources* **2016**, *327*, 44–55.

Manuscript received: February 7, 2019  
 Revised manuscript received: March 9, 2019  
 Accepted article published: March 11, 2019  
 Version of record online: March 26, 2019